Manuscript File Click here to view linked References

Corrosion damage detection in reinforced concrete using Rayleigh wave-based method

Weixia Cheng[a], Hai-Han Sun[a,b], Li Soon Wan[c,d], Zheng Fan[a,*], Kang Hai Tan[c,*]

[a]*School of Mechanical and Aerospace Engineering, Nanyang Technological University, 50 Nanyang Avenue, Singapore*
[b]*Now at Department of Electrical & Computer Engineering, University of Wisconsin-Madison, 1415 Engineering Dr, Madison, WI 53706, US*
[c]*School of Civil and Environmental Engineering, Nanyang Technological University, 50 Nanyang Avenue, Singapore*
[d]*Kajima Technical Research Institute Singapore, Singapore*

Abstract

Corrosion of reinforcing bars is a dominant cause of degradation of reinforced concrete (RC) structures. Over time, expansive products of corrosion build up tensile stresses within the concrete, leading to cracks on the exterior surface and spalling of concrete cover. To extend the service life of RC structures, a reliable non-destructive inspection method is required to detect and evaluate corrosion-induced internal cracks in concrete before spalling, so that timely repair can be conducted. Ultrasonic Rayleigh waves have been employed to detect near-surface cracks in concrete based on their transmission coefficient in frequency domain or their time-of-flight information. However, due to heterogeneity of concrete materials, the ill-defined Rayleigh wave component and the sensor coupling on the rough surface of concrete have a significant influence on accuracy of the method. In this study, an improved method using Rayleigh waves has been investigated to detect corrosion-induced internal cracks in concrete. In the method, energy spectrum of the Rayleigh wave is analysed using the continuous wavelet transform and correlated to locations of internal cracks. This method is not sensitive to surface roughness of concrete members and does not need accurate identification of the Rayleigh wave components. Performance of the method was examined using corroded RC specimens with different cover depths and aggregate sizes. As a comparison,

*Corresponding author
Email addresses: ZFAN@ntu.edu.sg (Zheng Fan), ckhtan@ntu.edu.sg (Kang Hai Tan)

electrochemical tests were performed to map the corrosion current density. The test results showed very good agreement with the corrosion damage map generated from the proposed Rayleigh wave-based method.

Keywords: Reinforced concrete, Rayleigh wave, corrosion-induced cracks, continuous wavelet transform (CWT)

---

1. Introduction

Reinforced concrete (RC) is the most widely used construction building material. Although RC is a durable material, corrosion of reinforcing bars is the main reason for its deterioration. In corroded RC members, expansive corrosion products forming on the reinforcing bars generate internal tensile stresses. When these stresses exceed tensile strength of concrete, internal cracks will form, resulting in spalling of concrete. Partial delamination of concrete cover leads to impairing the strength and durability of the RC structures [1–3]. Therefore, an effective non-destructive method that can detect corrosion damage in concrete before the occurrence of spalling is crucial for health monitoring of RC structures [4].

In this regard, non-destructive inspection techniques to evaluate corrosion damage in RC structures have been extensively investigated in recent decades. They can be broadly classified into electrochemical, electromagnetic, and ultrasonic methods [5–8]. Traditional electrochemical methods for corrosion evaluation include half-cell potential measurements [9, 10], electrochemical impedance spectroscopy [11–13], polarization resistance measurements [14–16], and galvanostatic pulse method [17, 18]. These inspection methods typically require drilling holes in concrete to connect electrical wires to the reinforcing bar. To measure corrosion rate without physical connections to reinforcing bars, an electrical pulse response analysis method with a four-probe Wenner array has been proposed [19]. Although the method has been widely used to assess corrosion damage in bridges, it is less effective when evaluating corrosion condition of RC slabs with paint, as they need to be removed [20, 21]. Several studies have investigated the possibility of applying electromagnetic (EM) waves for detecting corroded areas [22–27]. Since corroded reinforcing bars reflect less EM waves compared to non-

corroded ones, the EM method generates reflection amplitude maps, which can be correlated with the corroded areas. It should be noted that environmental conditions such as concrete surface anomalies, moisture in concrete, and reinforcing bar configurations can also affect reflection amplitude of EM waves, thereby compromising reliability of the method [28–31].

Ultrasonic Rayleigh waves, which propagate along the surface of solid materials, have been demonstrated to be useful in the characterisation of near-surface cracks [32–35], which can be used as indicators of corrosion damage in concrete [36]. Nonlinear Rayleigh wave methods have been investigated to detect micro-damage in concrete using the acoustic nonlinearity parameter [37–39]. However, the accuracy of these methods can be significantly influenced by various environmental parameters such as temperature and humidity [39]. Much research has also focused on exploring linear Rayleigh waves to detect and characterize near-surface cracks in concrete. It has been proposed that the time-of-flight of transmitted Rayleigh waves can be used to determine the depth of cracks [40, 41]. However, this method does not perform well when applied to actual cracks in concrete with ill-defined tips [40]. For such cracks, transmission coefficients have been investigated and correlated with normalized crack depths [33, 42–44]. Ultrasonic arrays were also developed to detect subsurface cracks in concrete using synthetic aperture focusing technique [45–48]. It should be noted that the methods based on time-domain signals suffer from common issues such as heterogeneous properties of the concrete material, incoherent signal noise, and transducer coupling on rough surface of concrete members [33, 43]. To mitigate these issues, methods based on frequency-domain signals were investigated. Cut-off frequencies of transmitted Rayleigh waves were explored to estimate the depth of surface-breaking cracks [49]. To avoid spectral leakage, this method requires accurate separation of transmitted Rayleigh waves from other elastic waves [50, 51]. However, in reality, it would be challenging to distinguish the components of Rayleigh waves accurately, due to complex material properties in concrete that would cause additional scattering of ultrasonic bulk waves [52].

Motivated by the issues outlined above, the energy spectrum of transmitted Rayleigh waves based on the continuous wavelet transform (CWT) is analysed and correlated

with corrosion-induced internal cracks. This method does not require accurate identification of Rayleigh wave components, and thus it is easier to be applied in practice. A pair of dry-point-contact (DPC) transducers is used to scan corroded RC specimens, which is not sensitive to concrete surface conditions. The central frequency is identified in the spectrum of transmitted Rayleigh waves in each scan, which could indicate the presence and severity of corrosion-induced cracks. Given that the cracks only exist in a small region near the reinforcing bars, they would affect a small portion of the spectrum from the scan. Therefore, the median of the central frequencies collected in all the scans is used as the baseline of comparison. Then the ratio of central frequency collected at each scan with respect to the median of the dataset is obtained, and correlated to the severity of corrosion-induced damage at this location. Electrochemical measurements of corrosion current density are performed to verify the performance of the proposed method, and excellent agreement is obtained between them.

The remaining paper is arranged as follows. Section 2 describes the experimental setup, including the sample preparation, accelerated corrosion tests, and ultrasonic measurements. Details of the proposed method are given in Section 3, while test results under different cover depths and aggregate sizes are presented in Section 4. Finally, Section 5 presents the findings.

2. Experimental programme

2.1. Specimen preparation

Three RC specimens S#1 - S#3 with dimensions of 500 mm $\times$ 400 mm $\times$ 100 mm were prepared. Each sample had three embedded steel round bars with 10 mm diameter. The mix proportions for the concrete specimens are summarized in Table 1. Specimens S#1 and S#2 shared the same aggregate size, but had cover depths of 25 mm and 30 mm, respectively. Specimens S#2 and S#3 had the same cover depth, but with the maximum aggregate size of 10 mm and 25 mm, respectively, which are within the typical range of aggregates used in RC structures of buildings [53]. These samples were used to investigate the influence of cover depth and aggregate size on the performance of the proposed method. The specimens were cast in wooden molds, demolded after 24

hours, and cured for another 27 days before being subjected to accelerated corrosion tests.

Table 1

Mix proportions for concrete with three reinforcing bar of 10 mm diameter.

Specimen no.	Cover depth (mm)	*w*/*c*	Unit:kg/m^3			
			Cement 42.5 N	Water	Fine aggregate	Coarse aggregate
S#1	25	0.53	468.5	247.6	747	936.9 (8-10 mm)
S#2	30	0.53	468.5	247.6	747	936.9 (8-10 mm)
S#3	30	0.53	495.5	262.6	600	1021.9 (5-25 mm)

2.2. Accelerated corrosion process

The RC samples were subjected to an accelerated corrosion test to produce corrosion damage, as shown in Fig. 1. In the experiment, reinforcing bars R1 and R3 were subjected to accelerated corrosion, while R2 served as the reference reinforcing bar without corrosion. Plastic containers without any bottom were adhesively bonded to the concrete surface at locations above R1 and R3. The containers were filled with sodium chloride (NaCl) of 5% concentration as an electrolyte. The DC power source (Keysight N6701A) applied a constant voltage of 20 V to R1 and R3 that were connected to positive channels 1 and 2 as anodes. Copper plates were immersed in the NaCl solution as cathodes and connected to negative channels 1 and 2. The concrete specimens were corroded for two weeks before ultrasonic measurements were taken. It should be noted that the accelerated corrosion using impressed current is not entirely representative of natural corrosive environments. This can lead to varying corrosion patterns around reinforcing bars [54].

2.3. Ultrasonic measurements

Fig. 2 shows the configuration of the ultrasonic scanning to detect corrosion-induced cracks in concrete. A pair of 50 kHz longitudinal wave dry-point-contact (DPC) transducers (S1844 ACS) spaced 16 mm apart was placed directly on the surface of the

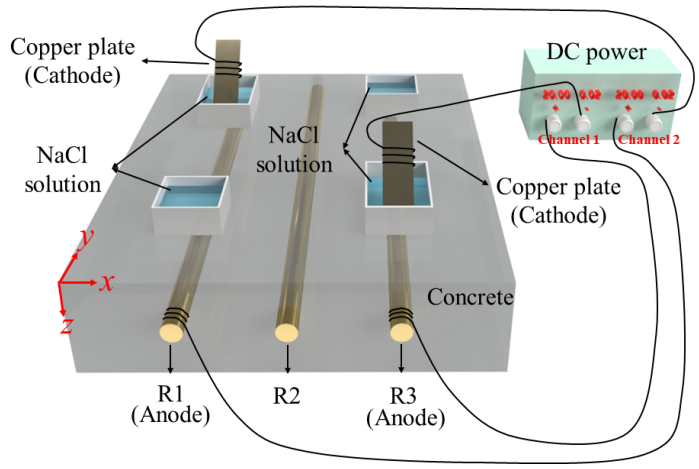

Fig. 1. Accelerated corrosion test setup. Reinforcing bars R1 and R3 were subjected to accelerated corrosion, and R2 was left as the reference without corrosion.

concrete structure to transmit and receive signals. This setup was employed to differentiate the Rayleigh wave from other wave components, such as the reflection from the bottom. It should be noted that acrylic holders were used to enclose the transducer and create a 1 mm gap, thereby preventing wave propagation through the air. A high-power computer-controlled ultrasonic system (RITEC RAM-5000) was used to generate a one-cycle Hann-windowed tone-burst signal with a central frequency at 50 kHz. The selection of the central frequency involves striking a balance between reducing the influence of aggregate scattering on the transmitted Rayleigh wave spectrum, ensuring that the corresponding wavelength exceeds the cover depths of the tested samples, and maintaining sensitivity to corrosion-induced cracks. It is worth noting that the velocity of Rayleigh waves was measured to be 2124 m/s in this experiment, corresponding to a wavelength of 42 mm at a frequency of 50 kHz. Given that the wavelength is smaller than the thickness of specimens (100 mm) and larger than the maximum aggregate size of 25 mm, it is expected that the wave velocity remains constant throughout the utilized frequency range [55–57]. The received signals were then digitized using an os-

cilloscope (Lecroy HDO6054) at a sampling frequency of 25 MHz with a time window of 100 μs. Figure 2 shows the scanning grid lines for the placement of the source and receiver on the concrete surface. To unambiguously differentiate between corroded and healthy regions in the testing samples, signals at 40×14 positions were measured in a grid of 8 mm in the x-direction, and 32 mm in the y-direction, covering an area of 320 mm by 448 mm. An even finer resolution could be achieved by acquiring signals in a smaller scanning step, which could be beneficial in other RC setups. In addition, the scanning test was repeated three times. The mean signals were subsequently processed to reduce deviations caused by measurement noise.

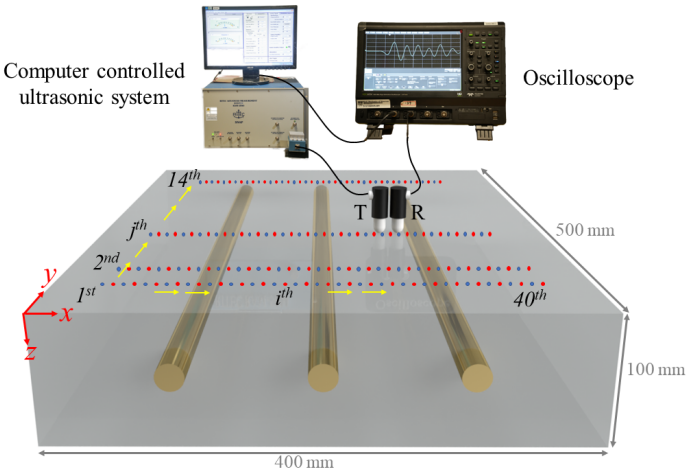

Fig. 2. Rayleigh wave scanning test setup. A pair of DPC transducers was used to transmit and receive signals.

3. Rayleigh wave-based inspection methodology

Upon acquiring the ultrasonic signals in Section 2.3, a method was proposed to process these data for corrosion damage evaluation. It involved three steps: the continuous wavelet transform (CWT) was performed on the acquired signals to obtain the distribution of wavelet transform coefficients over time and frequency. Subsequently, the energy spectrum of the transmitted Rayleigh wave was calculated. Finally, the central

frequency in the spectrum was analysed to map the corrosion damage.

3.1. Continuous wavelet transform (CWT)

The continuous wavelet transform (CWT) provides a balanced way of decomposing time-domain signals into a two-dimensional plot depicting amplitude as a function of both time and frequency [58]. It involves computing a set of wavelet coefficients W, which are the inner products of the signal and a wavelet basis, given by [59–61]:

$$W\{x(t); a, b\} = \int x(t)\psi^*_{a,b}(t)dt = \frac{1}{\sqrt{|a|}} \int x(t)\psi^*(\frac{t-b}{a})dt, \tag{1}$$

where $x(t)$ is the signal in time domain; $\psi_{a,b}(t)$ is the basic wavelet that serves as the prototype for generation of other window functions with dilation a and translation b, and (*) indicates complex conjugate operation; the constant $\frac{1}{\sqrt{|a|}}$ is used for energy normalization. In this study, the Morlet wavelet is used as the basic wavelet, as it is a sinusoidal function modulated by a Gaussian function and has characteristics similar to mechanical impulses [62–64].

3.2. Energy spectrum based on CWT

Following the calculation of wavelet coefficients W by Eq. (1), the power spectral density (PSD) E_f at a frequency f is derived by:

$$E_f = \int_0^{t_s} W^2 dt. \tag{2}$$

Here t_s is the end time of the Rayleigh wave, which is estimated by:

$$t_s = \frac{d}{v_R} + \frac{n_c}{f_c}, \tag{3}$$

where d denotes the spatial distance between the source and the receiver; v_R is the Rayleigh wave velocity, which is measured as 2128 m/s in this experiment; n_c and f_c are the number of cycles and the central frequency of the source wave, respectively. Furthermore, CWT is performed on the entire signals first, and then PSD is calculated over time. This eliminates the truncation effect of selecting a Rayleigh wave with an integral number of cycles.

3.3. Corrosion damage map

The method to generate a corrosion damage map was developed from observation of the energy spectrum of transmitted Rayleigh waves. Figure 3 illustrates the decay of energy of the Rayleigh waves at different frequencies and the corrosion-induced cracks. The energy of the Rayleigh waves reaches their maximum intensity at a depth of approximately 1/3 of the wavelength and then decays exponentially with depth [49, 65]. It is known that a typical corrosion-induced crack grows from the reinforcing bar towards the surface [66]. As shown in Fig. 3(a), when the depth of the crack tip, i.e. the distance from the crack tip to the surface of the material, exceeds 1/3 of the wavelength at the central frequency (f_c) of the source wave, the crack blocks more energy at low frequencies ($f_l < f_c$) than that at high frequencies ($f_h > f_c$). Therefore, it is expected that the central frequency of the Rayleigh wave passing through the crack would become higher.

Conversely, as shown in Fig. 3(b), in a more severely corroded region where the depth of the crack tip is less than 1/3 of the wavelength at f_c, the crack blocks most of the energy of the higher frequencies of the Rayleigh wave. The lower frequency component still has a significant amount of energy below the reinforcing bar and is less affected by the crack than the higher frequencies. Therefore, it is expected that the central frequency of the transmitted Rayleigh wave would become lower when the crack tip is closer to the concrete surface. Consequently, it would be possible to correlate the severity of the corrosion damage, which can be indicated by the depth of the crack tip, with the relative change in the central frequency. It is noteworthy that the spectrum change in transmitted Rayleigh wave signals is dominantly affected by the projected length of a crack in the vertical direction, regardless of its width and tilted angle. This also suggests that it would not be possible to reconstruct the shape of the crack by the current method.

This method is demonstrated by the accelerated corrosion test presented in Fig. 1. Figure 4 compares the energy spectrum of transmitted Rayleigh waves received at point 10 of line 1 (near R1) from concrete specimen S#1 before and after the accelerated corrosion. It can be seen that the central frequency in the spectrum of transmitted Rayleigh waves with corrosion (58.42 kHz) is lower than that without corrosion (62.62

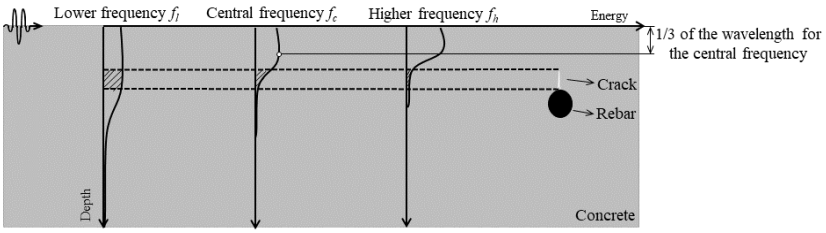

(a)

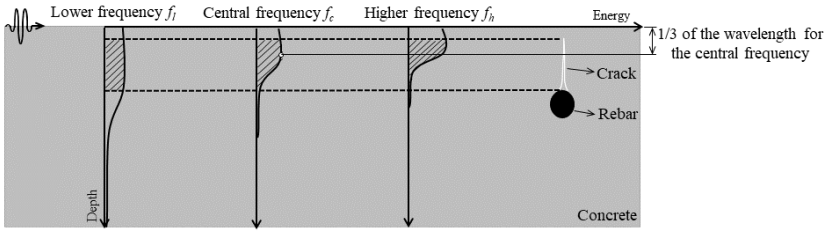

(b)

Fig. 3. Schematics of attenuated energy at different frequencies of Rayleigh waves while reaching corrosion-induced cracks with (a) depth of crack tip exceeding 1/3 of the wavelength; (b) depth of crack tip less than 1/3 of the wavelength. Shaded areas indicate the amount of energy blocked by a crack.

kHz).

It should be pointed out that practically it is not feasible to take the measurements when the structure is in initial and pristine condition. Therefore, in this work, a reference-free method is proposed to determine the threshold of corrosion damage. It is well-established that corrosion initially occurs surrounding the reinforcing bar. Consequently, only the spectrum of transmitted waves acquired in the proximity of reinforcing bars will be impacted by corrosion-induced cracks. This represents a small fraction of all the scanned data. Therefore, the median of the central frequency in all testing points is selected as the baseline for the corrosion-free measurement. To demonstrate the consistency of the proposed method at different locations, ultrasonic measurements were taken at all 40×14 locations on each specimen, and the results were post-processed in the frequency domain to obtain the central frequency at each

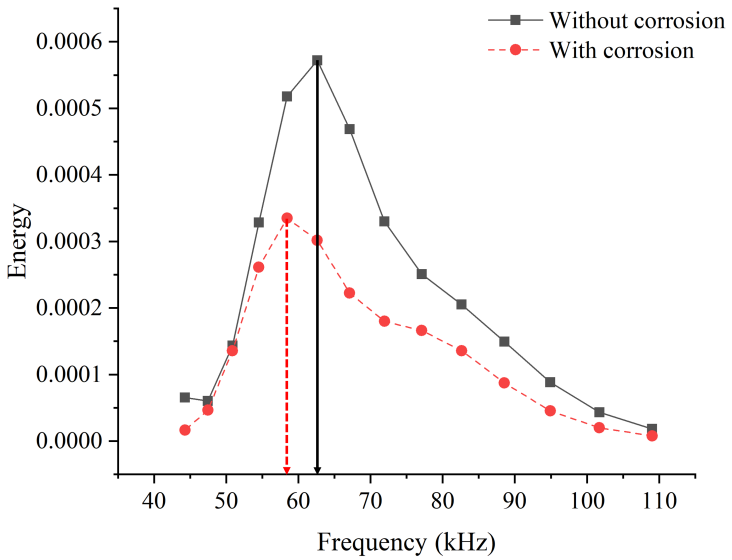

Fig. 4. Energy spectrum transformed from Rayleigh wave recorded at point 10 of line 1 before and after accelerated corrosion process for specimen S#1, as indicated by a black solid line and a red dash line, respectively.

location. It should be noted that when conducting ultrasonic scanning tests on laboratory or field samples, it is essential to ensure that the length of the scan in the direction perpendicular to the reinforcing bar exceeds the bar spacing. This measurement can provide a reliable median of central frequency as a benchmark for comparison. Table 2 presents the central frequency distribution of all the scanning data acquired from specimens before and after the accelerated corrosion. Among the 40×14 sets of the central frequency distribution for specimens S#1 and S#2 before accelerated corrosion, over 99% of the data sets have the same central frequency, with only less than 1% of the data sets having a slightly lower central frequency. This is believed to be related to the connected voids in concrete structures, which is inherent in concrete structures. Specimen S#3 with large aggregate size has 93% of data sets with the same central frequency, while 7% of data sets have slightly higher central frequencies, most likely due to scattering from large aggregates. After the accelerated corrosion, a small portion

of the spectrum was impacted by corrosion-induced cracks appearing in the vicinity of reinforcing bars, resulting in shifts of the central frequency from 62.62 kHz to other frequencies. Nevertheless, the median central frequency value of 62.62 kHz was observed to remain constant, serving as the baseline for comparison.

Table 2

Central frequency distribution of 560 sets of scans before and after accelerated corrosion.

Corrosion condition	Specimen	Number of scans with f_c at 62.62 kHz	Number of scans with other f_c
Without corrosion	**S#1**	556	4
	S#2	556	4
	S#3	522	38
Corrosion	**S#1**	492	68
	S#2	453	107
	S#3	475	85

Note that small cracks with depths of the tips exceeding 1/3 of the wavelength as well as large aggregates can both cause frequencies to be higher than the median, and it is difficult to distinguish the two. Accordingly, our proposed method focuses exclusively on detecting corrosion-induced cracks with the depth of crack tips less than 1/3 of the wavelength, approximately 14 mm in this experiment. It should be noted that the spacing between transducers should be larger than 1/3 of the wavelength of the Rayleigh wave, and it is chosen to be 16 mm in this work.

The flowchart for generating a corrosion damage map using the proposed method is shown in Fig. 5. It begins with processing each A-scan acquired from the specimens to calculate its energy spectrum based on Eq. (1) and Eq. (2). The central frequencies in the spectrum of all the Rayleigh wave signals in the scan are extracted, and the median of these central frequencies is obtained. The ratio between the central frequency of a single A-scan f_i and the frequency median f_m is computed as R_{fi} (f_i / f_m), and this is used to map the corrosion damage at different locations in the structure.

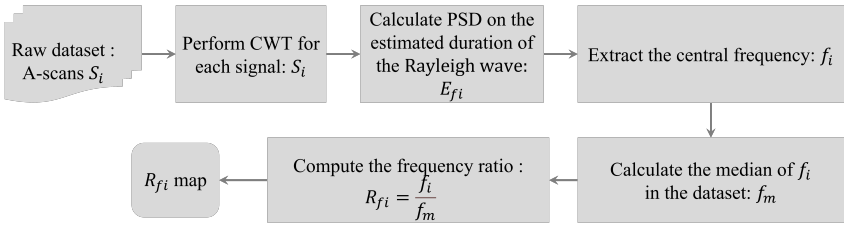

Fig. 5. Flowchart to obtain corrosion damage map for an RC specimen using the proposed method.

4. Results

The proposed methodology was implemented in the evaluation of three RC specimens before and after the accelerated corrosion process. Several cross-sectional crack patterns were analysed and correlated to the frequency ratio. Additionally, the three corroded specimens were also examined using the electrochemical methods to assess and validate the proposed methodology.

4.1. Ultrasonic measurement results

Ultrasonic measurements were conducted on the RC specimens before and after accelerated corrosion, following the procedure described in Section 2.3. Figure 6(a) shows the corrosion damage maps generated by the proposed method with non-corroded specimens. The scale color represents the ratio of the central frequency in the spectrum to the median in the dataset R_{fi}. As stated in Section 3.3, corrosion-induced internal cracks with the depth of the tips less than 1/3 of the wavelength can lead to a lower central frequency in the transmitted Rayleigh wave. Therefore, we use (R_{fi} =1) as the maximum value in the colorbar to represent the results. As can be observed in the corrosion damage map of non-corroded specimen S#3, the central frequencies are equal to or greater than the median value due to the scattering from the large aggregates. For the non-corroded specimens S#1 and S#2, the central frequencies in most regions are equal to the median. The unusual points (shown in light blue color) are due to the presence of large and connected voids caused by imperfect casting. Connected voids and internal cracks have similar effects on ultrasound waves, so it is challenging to distinguish

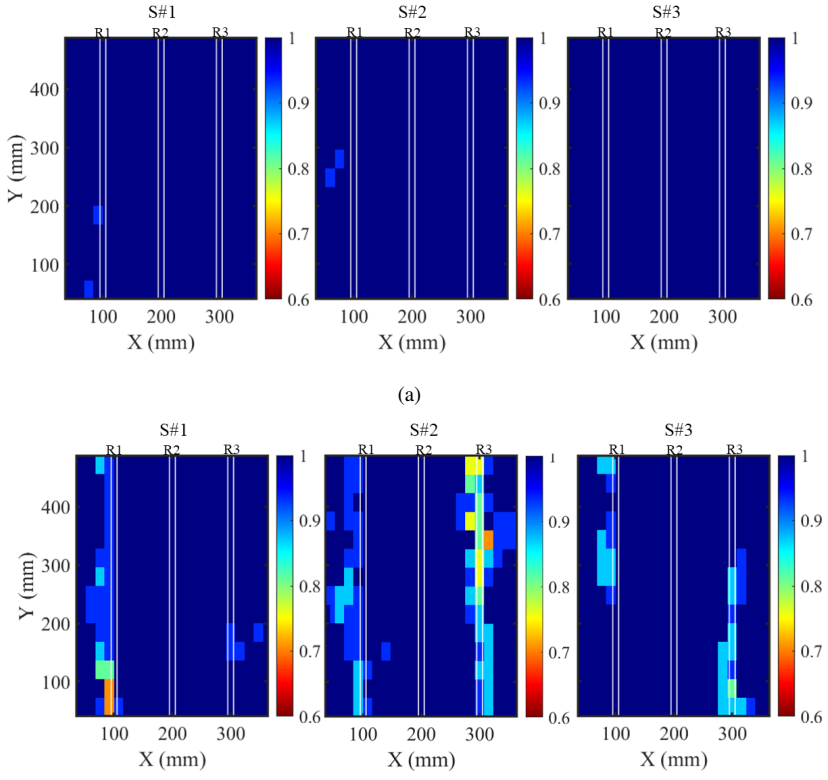

Fig. 6. Corrosion damage maps that depict the frequency ratio (R_{fi}) for three RC specimens with different cover depths and aggregate sizes: (a) before accelerated corrosion; (b) after accelerated corrosion.

them. Nonetheless, the detection of connected voids is also important, since oxygen, water, and carbon dioxide can easily enter the concrete medium and cause corrosion, if these voids are close to the reinforcing bar.

The corrosion damage maps of the three RC specimens subjected to accelerated corrosion are shown in Fig. 6(b). The R_{fi} values smaller than 1, indicating a downshift in the central frequency, appear at locations near R1 and R3 on all specimens. This corresponds well with the fact that only R1 and R3 experienced corrosion. It can be seen that the unusual points of S#2 in Fig. 6(a) undergo a shift towards a cyan-blue hue

after accelerated corrosion, indicating a reduced frequency ratio. This alteration can be attributed to the appearance of corrosion-induced cracks. The regions around R2 have R_{fi} values greater than or equal to 1, suggesting there is no corrosion damage on R2. This also agrees well with the experimental setup where R2 was the corrosion-free reference bar.

4.2. Crack pattern analysis

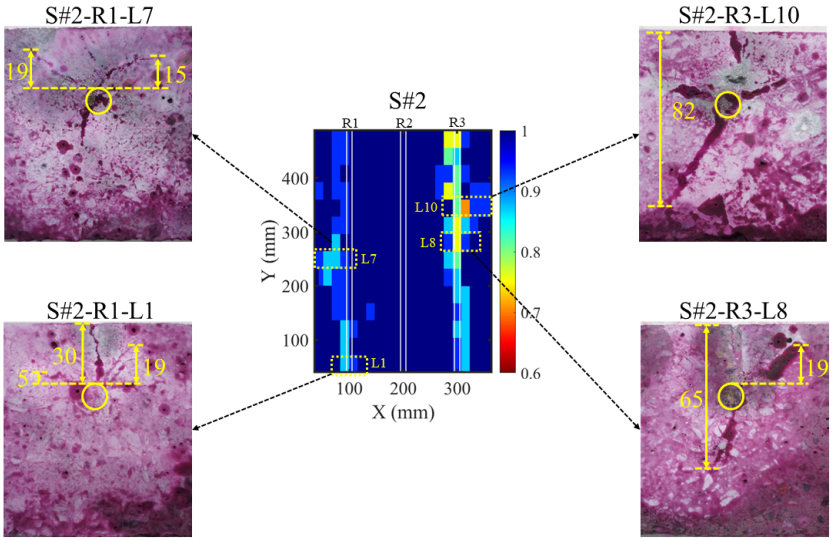

Fig. 7. Dye penetrant crack patterns on different cross-sections of specimen S#2.

To examine patterns of corrosion-induced cracks, a dye penetrant inspection method was carried out on several cross-sections along the measurement lines. Cracks will appear as visible red lines on the cross-sectional surfaces [67]. Figure 7 shows the crack patterns on different cross-sections of specimen S#2. It can be found that the central frequency drop occurs when the distance between the crack tip and the surface is within 15 mm, approximately 1/3 of the wavelength of the Rayleigh wave generated in the experiment (14 mm). It can be seen that larger cracks correspond with smaller frequency ratios. This is because when cracks extend further, lower frequencies with corresponding longer wavelengths will be affected. It should be noted that in the case

of multiple cracks, which typically happen in reality, the largest vertical length covered by all cracks will be indicated by the frequency ratio.

4.3. Validation of the proposed approach

To evaluate the effectiveness of the proposed method, electrochemical tests were conducted with potentiostat equipment SP-300. The test setup is illustrated in Fig. 8. Polarization resistance (R_p) was measured by using a three-electrode system, including a $Cu/CuSO_4$ reference electrode, a stainless steel sheet with a size of 150 mm × 150 mm as a counter electrode, and a reinforcing bar embedded in concrete as a working electrode. The corrosion current density I_{corr}, indicating the corrosion levels, was calculated by using Stern and Geary's equation [68]:

$$I_{corr} = \frac{\beta_a \beta_c}{2.303(\beta_a+\beta_c)} \frac{1}{R_p} = \frac{B}{R_p}. \tag{4}$$

Here R_p denotes polarization resistance; β_a and β_c represent the anodic and cathodic slopes of the Tafel curve, respectively. A constant B value of 26 mV is adopted in this study [14].

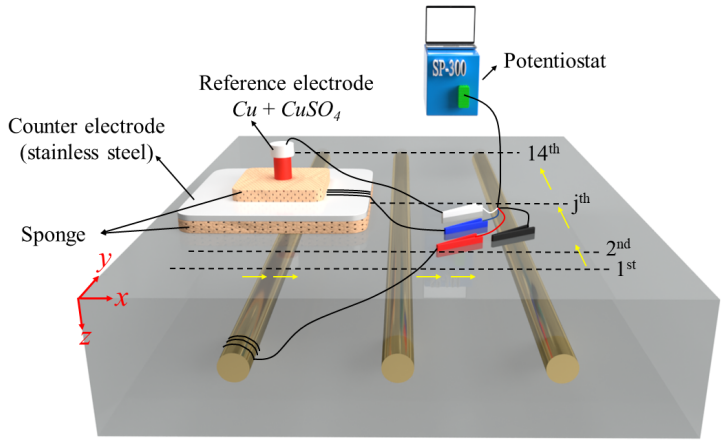

Fig. 8. Electrochemical test setup. Polarization resistance R_p was measured with a three-electrode system, including a $Cu/CuSO_4$ reference electrode, a 150 × 150 mm stainless steel sheet as a counter electrode, and a reinforcing bar as a working electrode.

Electrochemical measurements were required to be carried out over the three reinforcing bars. As a result, the imaging resolution in the x-direction was set to 100 mm, which is different from the ultrasonic imaging resolution of 8 mm. The reference electrode was manually moved along 14 cross-section lines along the y-direction at a step of 32 mm, as shown in Fig. 8. It should be noted that the resolution of It is noted that the electrode was moved along the x-direction first, followed by the y-direction. By doing so, the accuracy of the measurements was improved as successive tests performed at small intervals on the same reinforcing bar were avoided.

Figure 9 shows the corrosion current density maps obtained by the linear polarization resistance method. Table 3 provides the criteria for corrosion assessment based on interpretations of corrosion current density [2]. Referring to the table, the corrosion current density readings are greater than 0.1 $\mu A/cm^2$, both of which indicate that R1 and R3 are actively corroding. It is in accordance with the actual corrosion situations. As can be seen from the corrosion current maps in Fig. 9, for S#1, R1 exhibits corrosion throughout the bar length while R3 exhibits the most severe corrosion in the middle area. Specimen S#2 exhibits the most severe corrosion at the lower-left and upper-right corners, while S#3 shows the most severe corrosion at the upper-left and lower-right corners. Compared to the corrosion damage maps generated by Rayleigh wave-based methods shown in Fig. 6(b), the areas with mild corrosion and severe corrosion agree very well. However, there is some variability in some specific points between these two methods. This is because electrochemical measurements provide an average corrosion current density for the specific area of the reinforcing bar covered by the current flow [17], whereas ultrasonic measurements capture corrosion damage at each point along the reinforcing bar by collecting signals in smaller increments. The proposed ultrasonic method provides more precise and detailed corrosion information for the tested areas compared to electrochemical methods.

5. Conclusion

The paper presents a reference-free method for detecting corrosion-induced cracks in concrete structures. The energy spectrum of transmitted Rayleigh waves is gener-

Table 3

Criteria for corrosion of steel in concrete for corrosion current density [2].

Corrosion current density	Corrosion condition
I_{corr} <0.1 $\mu A/cm^2$	Passive condition
I_{corr} 0.1-0.5 $\mu A/cm^2$	Low to moderate corrosion
I_{corr} 0.5-1 $\mu A/cm^2$	Moderate to high corrosion
I_{corr} > 1 $\mu A/cm^2$	High corrosion rate

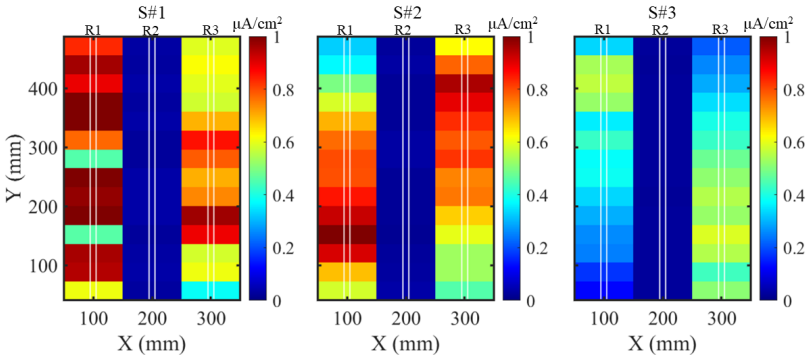

Fig. 9. Corrosion current density maps for corroded RC specimens.

ated based on the continuous wavelet transform (CWT). The central frequency at each scanning location is obtained and compared with the median of central frequencies at all locations. Their relative ratio indicates the severity of corrosion-induced cracks. It shows that cracks with depths of tips less than 1/3 of the wavelength can be reliably detected by this method. Larger cracks correspond with smaller frequency ratios. To verify the proposed method, electrochemical tests were carried out to map the corrosion current density. The areas with a decreased central frequency are consistent with the corroded areas obtained from corrosion current density maps, and the areas with mild and severe corrosion also agree very well. Furthermore, due to the high efficiency of signal processing, the proposed methodology is suitable for large-scale data processing to map corrosion damage on RC structures.

It should be noted that this method is inadequate for measuring the width and angle

of cracks, which can also be potential indicators of corrosion severity. Additionally, this method is not reliable for detecting corrosion-induced cracks in the initial stage, when the distance between the tip of the crack and the surface is larger than 1/3 of the wavelength of the applied Rayleigh wave. Accurate detection of such cracks requires further investigation. Furthermore, there is a notable disparity in corrosion patterns around reinforcing bars induced by the impressed current technique compared to those from natural corrosion. Therefore, evaluating corrosion damage resulting from naturally corrosive environments in the future would be useful. Moreover, future investigations will explore the integration of electrochemical and ultrasonic methods for quantifying corrosion damage in RC structures.

Acknowledgments

The authors acknowledge funding from National Research Foundation, Singapore, and Ministry of National Development, Singapore, under its Cities of Tomorrow R&D Programme (CoT Award No. COT-V2-2019-1).

References

[1] J. G. Cabrera, Deterioration of concrete due to reinforcement steel corrosion, Cem. Concr. Compos. 18 (1) (1996) 47–59.

[2] J. P. Broomfield, Corrosion of steel in concrete: understanding, investigation and repair, CRC Press, 2003.

[3] C. Fang, K. Lundgren, L. Chen, C. Zhu, Corrosion influence on bond in reinforced concrete, Cem. Concr. Res 34 (11) (2004) 2159–2167.

[4] D. M. McCann, M. C. Forde, Review of NDT methods in the assessment of concrete and masonry structures, NDT E Int. 34 (2) (2001) 71–84.

[5] S. Ahmad, Reinforcement corrosion in concrete structures, its monitoring and service life prediction—-a review, Cem Concr Compos 25 (4-5) (2003) 459–471.

[6] S. K. U. Rehman, Z. Ibrahim, S. A. Memon, M. Jameel, Nondestructive test methods for concrete bridges: A review, Constr Build Mater. 107 (2016) 58–86.

[7] J. Zhang, M. Zhang, B. Dong, H. Ma, Quantitative evaluation of steel corrosion induced deterioration in rubber concrete by integrating ultrasonic testing, machine learning and mesoscale simulation, Cem Concr Compos 128 (2022) 104426.

[8] A. Sharma, S. Sharma, S. Sharma, A. Mukherjee, Monitoring invisible corrosion in concrete using a combination of wave propagation techniques, Cem Concr Compos 90 (2018) 89–99.

[9] C. ASTM, Standard test method for half-cell potentials of uncoated reinforcing steel in concrete (1999).

[10] B. Elsener, C. Andrade, J. Gulikers, R. Polder, M. Raupach, Half-cell potential measurements—potential mapping on reinforced concrete structures, Mater. Struct. 36 (7) (2003) 461–471.

[11] P. Gu, S. Elliott, R. Hristova, J. Beaudoin, R. Brousseau, B. Baldock, A study of corrosion inhibitor performance in chloride contaminated concrete by electrochemical impedance spectroscopy, ACI Mater. J. 94 (1997) 385–395.

[12] S. Ford, J. Shane, T. Mason, Assignment of features in impedance spectra of the cement-paste/steel system, Cem Concr Res 28 (12) (1998) 1737–1751.

[13] O. Poupard, A. A¨ıt-Mokhtar, P. Dumargue, Corrosion by chlorides in reinforced concrete: Determination of chloride concentration threshold by impedance spectroscopy, Cem Concr Res 34 (6) (2004) 991–1000.

[14] C. Andrade, J. Gonz´alez, Quantitative measurements of corrosion rate of reinforcing steels embedded in concrete using polarization resistance measurements, Materials and corrosion 29 (8) (1978) 515–519.

[15] K. C. Clear, Measuring rate of corrosion of steel in field concrete structures, Transp. Res. Rec. (1211) (1989).

[16] C. Andrade, M. C. Alonso, J. A. Gonzalez, An initial effort to use the corrosion rate measurements for estimating rebar durability, Corrosion rates of steel in concrete, ASTM STP 1065 (1990) 29–37.

[17] C. Newton, J. Sykes, A galvanostatic pulse technique for investigation of steel corrosion in concrete, Corros. Sci. 28 (11) (1988) 1051–1074.

[18] S. Sathiyanarayanan, P. Natarajan, K. Saravanan, S. Srinivasan, G. Venkatachari, Corrosion monitoring of steel in concrete by galvanostatic pulse technique, Cem Concr Compos 28 (7) (2006) 630–637.

[19] J. Yu, A. Sasamoto, M. Iwata, Wenner method of impedance measurement for health evaluation of reinforced concrete structures, Constr Build Mater. 197 (2019) 576–586.

[20] L. Sadowski, Methodology for assessing the probability of corrosion in concrete structures on the basis of half-cell potential and concrete resistivity measurements, Sci. World J. 2013 (2013).

[21] R. Du Plooy, S. P. Lopes, G. Villain, X. Derobert, Development of a multi-ring resistivity cell and multi-electrode resistivity probe for investigation of cover concrete condition, NDT E Int. 54 (2013) 27–36.

[22] S. Hong, W. W.-L. Lai, G. Wilsch, R. Helmerich, R. Helmerich, T. G¨unther, H.Wiggenhauser, Periodic mapping of reinforcement corrosion in intrusive chloride contaminated concrete with gpr, Constr Build Mater. 66 (2014) 671–684.

[23] L. Calabrese, L. Bonaccorsi, M. Galeano, E. Proverbio, D. Di Pietro, F. Cappuccini, Identification of damage evolution during scc on 17-4 ph stainless steel by combining electrochemical noise and acoustic emission techniques, Corros. Sci. 98 (2015) 573–584.

[24] M. Abouhamad, T. Dawood, A. Jabri, M. Alsharqawi, T. Zayed, Corrosiveness mapping of bridge decks using image-based analysis of gpr data, Autom. Constr. 80 (2017) 104–117.

[25] S. Hong, H. Wiggenhauser, R. Helmerich, B. Dong, P. Dong, F. Xing, Longterm monitoring of reinforcement corrosion in concrete using ground penetrating radar, Corros. Sci. 114 (2017) 123–132.

[26] P. T. Wong, W. W. Lai, J. F. Sham, C.-s. Poon, Hybrid non-destructive evaluation methods for characterizing chloride-induced corrosion in concrete, NDT E Int. 107 (2019) 102123.

[27] J. Qiu, H. Zhang, J. Zhou, W. Zhang, An smfl-based non-destructive quantification method for the localized corrosion cross-sectional area of rebar, Corros. Sci. 192 (2021) 109793.

[28] R. Parrillo, R. Roberts, A. Haggan, Bridge deck condition assessment using ground penetrating radar, Proceedings of the ECNDT, Berlin, German 2526 (2006) 112.

[29] A. Tarussov, M. Vandry, A. De La Haza, Condition assessment of concrete structures using a new analysis method: Ground-penetrating radar computer-assisted visual interpretation, Constr Build Mater. 38 (2013) 1246–1254.

[30] K. Dinh, N. Gucunski, J. Kim, T. H. Duong, Method for attenuation assessment of gpr data from concrete bridge decks, NDT E Int. 92 (2017) 50–58.

[31] K. Dinh, N. Gucunski, T. Zayed, Automated visualization of concrete bridge deck condition from gpr data, NDT E Int. 102 (2019) 120–128.

[32] C. Pecorari, Scattering of a rayleigh wave by a surface-breaking crack with faces in partial contact, Wave Motion 33 (3) (2001) 259–270.

[33] W.-J. Song, J. S. Popovics, J. C. Aldrin, S. P. Shah, Measurement of surface wave transmission coefficient across surface-breaking cracks and notches in concrete, J. Acoust. Soc. Am. 113 (2) (2003) 717–725.

[34] D. Aggelis, E. Leonidou, T. Matikas, Subsurface crack determination by onesided ultrasonic measurements, Cem Concr Compos 34 (2) (2012) 140–146.

[35] J. Xiao, J. Chen, X. Yu, D. Lisevych, Z. Fan, Remote characterization of surface slots by enhanced laser-generated ultrasonic rayleigh waves, Ultrasonics 119 (2022) 106595.

[36] V. S. Kuntal, P. Jiradilok, J. E. Bolander, K. Nagai, Estimating corrosion levels along confined steel bars in concrete using surface crack measurements and mesoscale simulations guided by model predictive control, Cem Concr Compos 124 (2021) 104233.

[37] G. Kim, E. Giannini, N. Klenke, J.-Y. Kim, K. E. Kurtis, L. J. Jacobs, Measuring alkali-silica reaction (asr) microscale damage in large-scale concrete slabs using nonlinear rayleigh surface waves, J. Nondestruct. Eval. 36 (2017) 1–6.

[38] D. E. Torello, J.-Y. Kim, J. Qu, L. J. Jacobs, Characterization of air-coupled ultrasonic receivers for nonlinear rayleigh wave nondestructive evaluation, J. Acoust. Soc. Am. 138 (3) (2015) 1837–1837.

[39] G. Kim, C.-W. In, J.-Y. Kim, K. E. Kurtis, L. J. Jacobs, Air-coupled detection of nonlinear rayleigh surface waves in concrete—application to microcracking detection, NDT E Int. 67 (2014) 64–70.

[40] Y. Lin, W.-C. Su, Use of stress waves for determining the depth of surfaceopening cracks in concrete structures, J. Mater. 93 (5) (1996) 494–505.

[41] T.-T.Wu, J.-S. Fang, P.-L. Liu, Detection of the depth of a surface-breaking crack using transient elastic waves, J. Acoust. Soc. Am. 97 (3) (1995) 1678–1686.

[42] D. Aggelis, T. Shiotani, D. Polyzos, Characterization of surface crack depth and repair evaluation using rayleigh waves, Cem Concr Compos 31 (1) (2009) 77–83.

[43] S.-H. Kee, J. Zhu, Using air-coupled sensors to determine the depth of a surface-breaking crack in concrete, J. Acoust. Soc. Am. 127 (3) (2010) 1279–1287.

[44] D. Aggelis, E. Kordatos, D. Soulioti, T. Matikas, Combined use of thermography and ultrasound for the characterization of subsurface cracks in concrete, Constr Build Mater. 24 (10) (2010) 1888–1897.

[45] D. Ghosh, S. Beniwal, A. Ganguli, A. Mukherjee, Reference free imaging of subsurface cracks in concrete using r ayleigh waves, Struct Control Health Monit 25 (10) (2018) e2246.

[46] D. Ghosh, R. Kumar, A. Ganguli, A. Mukherjee, Nondestructive evaluation of rebar corrosion–induced damage in concrete through ultrasonic imaging, J. Mater. Civ. Eng. 32 (10) (2020) 04020294.

[47] P. K. Mayakuntla, D. Ghosh, A. Ganguli, Classification of corrosion severity in concrete structures using ultrasonic imaging and linear discriminant analysis, Sustainability 14 (23) (2022) 15768.

[48] P. K. Mayakuntla, D. Ghosh, A. Ganguli, Nondestructive evaluation of rebar corrosion in concrete structures using ultrasonics and laser-based sensing, Nondestruct. Test. Eval. 37 (3) (2022) 297–314.

[49] G. Hevin, O. Abraham, H. Pedersen, M. Campillo, Characterization of surface cracks with rayleigh waves: a numerical model, NDT E Int. 31 (4) (1998) 289–297.

[50] M. Cerna, A. F. Harvey, The fundamentals of fft-based signal analysis and measurement, Tech. rep., Application Note 041, National Instruments (2000).

[51] S. W. Smith, Chapter 11 - fourier transform pairs, in: S. W. Smith (Ed.), Digital Signal Processing, Newnes, Boston, 2003, pp. 209–224.

[52] F.W. Lee, K. S. Lim, H. K. Chai, Determination and extraction of rayleigh-waves for concrete cracks characterization based on matched filtering of center of energy, J. Sound Vib. 363 (2016) 303–315.

[53] C. ASTM, et al., Standard specification for concrete aggregates, Philadelphia, PA: American Society for Testing and Materials (2003).

[54] S. Ahmad, Techniques for inducing accelerated corrosion of steel in concrete, Arab J Sci Eng 34 (2) (2009) 95.

[55] M. Goueygou, Z. Lafhaj, F. Soltani, Assessment of porosity of mortar using ultrasonic rayleigh waves, NDT E Int. 42 (5) (2009) 353–360.

[56] C.-W. In, J.-Y. Kim, K. E. Kurtis, L. J. Jacobs, Characterization of ultrasonic rayleigh surface waves in asphaltic concrete, NDT E Int. 42 (7) (2009) 610–617.

[57] T. Philippidis, D. Aggelis, Experimental study of wave dispersion and attenuation in concrete, Ultrasonics 43 (7) (2005) 584–595.

[58] D. S. Wilks, Chapter 10 - time series, in: D. S. Wilks (Ed.), Statistical Methods in the Atmospheric Sciences (Fourth Edition), fourth edition Edition, Elsevier, 2019, pp. 485–550.

[59] O. Rioul, M. Vetterli, Wavelets and signal processing, IEEE Signal Process Mag 8 (4) (1991) 14–38.

[60] C. Torrence, G. P. Compo, A practical guide to wavelet analysis, Bull Am Meteorol Soc 79 (1) (1998) 61–78.

[61] O. Rioul, P. Duhamel, Fast algorithms for discrete and continuous wavelet transforms, IEEE Trans. Inf. Theory 38 (2) (1992) 569–586. doi:10.1109/18.119724.

[62] B. Tang, W. Liu, T. Song, Wind turbine fault diagnosis based on morlet wavelet transformation and wigner-ville distribution, Renew. Energy 35 (12) (2010) 2862–2866.

[63] W. Lee, M. Ratnam, Z. Ahmad, Detection of chipping in ceramic cutting inserts from workpiece profile during turning using fast fourier transform (fft) and continuous wavelet transform (cwt), Precis. Eng. 47 (2017) 406–423.

[64] A. Silik, M. Noori, W. A. Altabey, R. Ghiasi, Z. Wu, Comparative analysis of wavelet transform for time-frequency analysis and transient localization in structural health monitoring, SDHM Struct. Durab. Health Monit. 15 (1) (2021) 1.

[65] Iv - equations, in: C.-O. Leiber, B. Dobratz (Eds.), Assessment of Safety and Risk with a Microscopic Model of Detonation, Elsevier Science, Amsterdam, 2003, pp. 41–78.

[66] P. Plucinski, Numerical analysis of stress distribution in concrete around corroding rebar, Procedia Eng. 108 (2015) 598–607. doi:10.1016/j.proeng.2015.06.185.

[67] S. Swartz, C. Go, Validity of compliance calibration to cracked concrete beams in bending, Experimental Mechanics 24 (2) (1984) 129–134.

[68] M. Stern, A. L. Geaby, Electrochemical polarization, J. Electrochem. Soc. 104 (1) (1957) 56.